



Faraday Discussions

**Variety, the spice of life and essential for robustness in
excitation energy transfer in light-harvesting complexes**

Journal:	<i>Faraday Discussions</i>
Manuscript ID	FD-ART-07-2019-000081.R1
Article Type:	Paper
Date Submitted by the Author:	02-Aug-2019
Complete List of Authors:	Oh, Sue Ann; University of Otago, Dodd-Walls Centre, Department of Physics Coker, David; Boston University, Department of Chemistry Hutchinson, David; University of Otago, Dodd-Walls Centre, Department of Physics

SCHOLARONE™
Manuscripts

Cite this: DOI: 00.0000/xxxxxxxxxx

Variety, the spice of life and essential for robustness in excitation energy transfer in light-harvesting complexes

Sue Ann Oh,^{a,b} David F. Coker,^c and David A. W. Hutchinson^{*a,d}

Received Date

Accepted Date

DOI: 00.0000/xxxxxxxxxx

For over a decade there has been some significant excitement and speculation that quantum effects may be important in the excitation energy transport process in the light harvesting complexes of certain bacteria and algae, in particular via the Fenna-Mathews-Olsen (FMO) complex. Whilst the excitement may have waned somewhat with the realisation that the observed long-lived oscillations in two-dimensional electronic spectra of FMO are probably due to vibronic coherences, it remains a question whether these coherences may play any important role. We review our recent work showing how important the site-to-site variation in coupling between chloroplasts in FMO and their protein scaffold environment is for energy transport in FMO and investigate the role of vibronic modes in this transport. Whilst the effects of vibronic excitations seem modest for FMO, we show that for bilin-based pigment-protein complexes of marine algae, in particular PC645, the site-dependent vibronic excitations seem essential for robust excitation energy transport, which may again open the door for important quantum effects to be important in these photosynthetic complexes.

1 Introduction

For over a decade there has been intense speculation regarding the potential role of quantum coherence in facilitating photosynthetic excitation energy transfer (EET). The impetus for this was the surprising discovery of long-lived oscillatory features (of the order of hundreds of femtoseconds) in the two-dimensional electronic spectra (2DES) of the Fenna-Mathews-Olsen (FMO) complex in the light-harvesting apparatus of green sulphur bacteria¹. Here, long-lived refers to a time scale far beyond that expected in a noisy, damp, disordered system and certainly long enough to plausibly influence the EET dynamics. Furthermore, a variety of systems such as the reaction centre for purple bacteria, the peripheral antenna complex LHCI from higher plants and the pigment-protein complexes (PPCs) of marine algae - phycoerythrin PE545 and phyococyanin PC645 - have also been observed to show the presence of long lived oscillations in their 2DES²⁻⁶.

But are these long-lived oscillations important in terms of the efficiency of EET in these systems? There is a growing consensus that the observed long-lived oscillatory spectral features are in

fact vibrational or vibronic in nature⁷⁻¹⁴. This raises questions as to whether these features can have any beneficial effect on EET. That said, it is still possible for vibronic effects to contribute to increased efficiency if they are perhaps inter-pigment in nature. Intramolecular modes that are of near-resonant frequency with energy gaps can bridge these gaps while promoting exciton delocalisation over the ground vibrational state of the donor and the excited vibrational state of the acceptor, leading to a resonant speed-up of EET providing vibronic enhancement.

In this paper, we briefly review our work¹⁵ showing that site-variation in the pigment-protein interactions in FMO are optimized to enhance EET and extend this treatment to include the role of vibronic modes. We note that the inclusion of these vibronic modes in FMO leads to perhaps modest effects, maybe due to the relatively small energy separation between individual exciton energies in FMO. We therefore go on to investigate the bilin-based phycobiliprotein PC645 and show that the effects are much more dramatic and possibly evolutionally significant in terms of the robustness of the EET pathways given the flexibility of the PPCs in marine algae.

2 Theoretical model

The total system-bath Hamiltonian is expressed as

$$\hat{H}_{tot} = \hat{H}_s + \hat{H}_b + \hat{H}_{sb}, \quad (1)$$

^a Dodd-Walls Centre for Photonic and Quantum Technologies, Department of Physics, University of Otago, Dunedin, New Zealand.

^b Institute of Physics, Charles University, CZ-121 16 Prague 2, Czech Republic.

^c Department of Chemistry, Boston University, Massachusetts 02215, USA.

^d Clarendon Laboratory, Department of Physics, University of Oxford, Oxford OX1 3PU, UK.

where \hat{H}_s , \hat{H}_b and \hat{H}_{sb} are the system (electronic), bath and system-bath interaction Hamiltonians respectively.

2.1 The electronic system

The electronic system consists of the chromophores in the pigment-protein complex (PPC). Its Hamiltonian is described by the tight-binding model in the site basis $|m\rangle$:

$$\hat{H}_s = \sum_{m=1}^N E_m |m\rangle \langle m| + \sum_{m \neq n}^N V_{mn} |m\rangle \langle n|, \quad (2)$$

where E_m , V_{mn} and N are the site energies, electronic coupling between pigments m and n and number of chromophores respectively. Since our system operates in a low-photon environment, the single exciton manifold approximation is valid here. The k th eigenstate of the system Hamiltonian (also known as the exciton state) can be decomposed in terms of the site basis:

$$|k\rangle = \sum_m c_{m,k} |m\rangle. \quad (3)$$

Initially, we use the 8-site FMO Hamiltonian for the *Prosthecochloris aestuarii* (*P. aestuarii*) species as presented by Moix et. al¹⁶.

2.2 The bath and system-bath coupling

The protein environment is modelled as a bath of harmonic oscillators with $\hat{H}_b = \sum_{i,m} \hbar \omega_{i,m} \left(b_{i,m}^\dagger b_{i,m} + \frac{1}{2} \right)$ where $b_{i,m}^\dagger$ ($b_{i,m}$) are the creation (annihilation) operators of excitations of the i th bath mode with frequency $\omega_{i,m}$ on pigment m . The phonon modes on each site are treated as being uncorrelated and coupled linearly to the diagonal part of the system Hamiltonian such that:

$$\hat{H}_{sb} = \sum_{i,m} u_{i,m} (b_{i,m}^\dagger + b_{i,m}) |m\rangle \langle m|. \quad (4)$$

Here $u_{i,m}$ is the coupling between the electronic transition of the m th site and the i th phonon mode. Physically, this equation reflects the effect of the protein environment dynamically modulating the site energies of the pigments. All information about the system-bath interaction of each pigment m is contained in its corresponding spectral density $J_m(\omega) = \pi \sum_i |u_{i,m}|^2 \delta(\omega - \omega_{i,m})$. The reorganization energy λ_m of pigment m is in turn related to $J_m(\omega)$ by the following integration over frequency ω :

$$\lambda_m = \frac{1}{\pi} \int_0^\infty \frac{J_m(\omega)}{\omega} d\omega. \quad (5)$$

3 Numerical methods

The numerical computation of the dynamics was performed using the Modified Redfield Theory (MRT)¹⁷ and its more recent upgrade, the Coherent Modified Redfield Theory (CMRT)¹⁸⁻²¹. Despite being perturbative, approximate methods, it has been shown that MRT and CMRT are reasonably valid over a broad range of system-bath coupling strengths and provide reasonable agreement with dynamics computed from numerically exact methods^{18,20,22}. This, coupled with the convenience and efficiency as compared to numerically exact methods, make them suitable

Table 1 Site-dependent reorganization energies λ_m and cutoff frequencies Ω_m of the FMO Drude-Lorentz spectral density used in this work.

m	λ_m (cm ⁻¹)	Ω_m (cm ⁻¹)
1	21.28	40.96
2	31.52	88.04
3	22.86	43.52
4	17.88	48.79
5	15.36	52.10
6	23.18	43.55
7	24.89	39.35
8	41.00	37.31

Mean 24.75 49.20

numerical methods in this work.

In contrast to MRT, CMRT allows the computation of coherence terms in the density matrix as well as the incorporation of some non-Markovianity, but at significant computational price. We thus employ MRT in most cases whilst using CMRT as a check for validity and where needed to calculate coherences. As in Refs.^{20,21}, we solve for the non-Markovian dynamics of CMRT with the non-Markovian Quantum Jump (NMQJ) technique^{23,24}. All computation is performed for the physiological temperature of $T = 300K$.

To aid physical interpretation, we represent the realistic spectral densities in the Drude-Lorentz regularized Ohmic form²⁵:

$$J_m^{DL}(\omega) = 2\lambda_m \Omega_m \frac{\omega}{\omega^2 + \Omega_m^2}, \quad (6)$$

where λ_m and Ω_m are the reorganization energy and cutoff frequency of site m respectively. Here the values of λ_m are calculated from the realistic site spectral densities via eq. 5. Ω_m , which corresponds to the inverse of the bath correlation time, can be obtained by first computing the site-dependent bath correlation function. For simplicity, we assume that the real part of the bath correlation functions can be represented by time decaying exponential functions, from which it is possible to extract the bath correlation time and subsequently Ω_m . We have verified that the dynamics with the realistic site-dependent spectral densities can be reliably reproduced with their Drude-Lorentz forms.

The computed values of λ_m and Ω_m for this model of the FMO complex are presented in Table 1. It is clear that the FMO complex has a fairly significant range of λ_m values where the largest is more than 2.5 times the magnitude of the smallest. It is interesting to note that the mean reorganization energy is also in a sense the most representative since half of the pigments have λ_m values close to this value.

The complexity of the problem is now significantly reduced since the spectral density is characterized by only two physically meaningful bath parameters, i.e. λ_m and Ω_m . Furthermore, we established that it is primarily the site variation in λ_m which modifies the dynamics, with very little contribution from the Ω_m site variation. Therefore, we present results for the Drude-Lorentz spectral density representation, keeping the site-dependent Ω_m fixed to the original configuration values in Table 1 and varying only λ_m .

4 Optimality of system-bath coupling configuration for FMO

We compared the energy transfer efficiency with the FMO site-dependent λ_m configuration to that from a large sample of random site-dependent λ_m configurations. We defined the energy transfer efficiency for a particular target site m , as obtained using the MRT formulation, in terms of the time-averaged population at the predominant exciton state of m :

$$\zeta_m = \frac{1}{\tau} \int_0^\tau P_k(t) dt, \quad (7)$$

where k is such that $|c_{m,k}|^2$ is maximal. Here P_k is the population in exciton state k , with $k = 1(2)$ for the target site $m = 3(4)$. The participation of an exciton state in each site is denoted by the absolute square of the corresponding expansion coefficient in eq. 3 and ranges from 0 to 1. Here $|c_{3,1}|^2 = 0.88$ and $|c_{4,2}|^2 = 0.59$. We have chosen $\tau = 1$ ps since a large portion of the relevant exciton dynamics and the experimentally observed oscillatory behaviour occur within this timescale. A higher value of ζ_m reflects a higher population transfer rate. Obviously, unlike the % efficiency figure of merit, ζ_m does not provide an intuitive gauge of efficiency when considered in isolation. Nevertheless, it is still useful for comparative purposes, which is sufficient. Also, based on existing knowledge of photosynthetic light-harvesting efficiency, we would expect the ζ_m value for at least the realistic λ_m configuration to correspond to a near 100% efficiency.

Two types of randomization were performed. In the first set, the efficiencies of all possible site permutations of the original λ_m configuration were computed with the efficiency of the actual FMO λ_m configuration falling in an impressive upper percentile range (85th and 78th percentile for the target sites of BChl 3 and 4 respectively)¹⁵. We then went on to show that this efficiency derived from differing coherent and incoherent pathways suggesting a plausible design principle for FMO which involves an effective interplay between the system and system-bath interaction. Energy transport mechanisms and pathways are combined with the fine tuning of pigment-protein interaction in such a way that the site-varying system-bath interaction strengths are efficiently exploited to optimise energy transport. Interestingly, it appeared that the mechanism for transport to BChl 3 was purely dissipative in nature and a simple funnelling process, whilst that to BChl 4 was seen to be at least partially coherent¹⁵, suggesting a more intriguing quantum role.

5 The vibronic system

In order to describe vibronic dynamics accurately, intramolecular vibrational modes must be explicitly included into the system Hamiltonian as opposed to treating them as part of the bath²⁶. This is because the slow vibrational relaxation of the intramolecular modes would lead to inaccuracies if subjected to the perturbative treatment of the bath. The incorporation of k selected vibrational modes into the electronic system is represented by the Holstein-like Hamiltonian^{27,28}

$$\hat{H}_s^v = \sum_m^N (E_m + \hbar \sum_j \omega_{m,j}^{vib} \nu_{m,j}) |m, \nu_m\rangle \langle m, \nu_m| + \sum_{m \neq n}^N J_{m, \nu_m; n, \nu_n} |m, \nu_m\rangle \langle n, \nu_n|, \quad (8)$$

where $|m, \nu_m\rangle = |m\rangle \otimes |\nu_{m,1}\rangle \otimes |\nu_{m,2}\rangle \cdots \otimes |\nu_{m,j}\rangle \cdots \otimes |\nu_{m,k}\rangle$ is the vibronic basis state. Here $\omega_{m,j}^{vib}$ and $\nu_{m,j}$ are the vibrational frequency and vibrational quantum number respectively of the vibrational mode j localized on pigment m . The coupling term is the electronic coupling modified by the Franck-Condon amplitudes and is given by

$$J_{m, \nu_m; n, \nu_n} = V_{mn} \langle \nu_{m,1}|0\rangle \langle \nu_{n,1}|0\rangle \langle \nu_{m,2}|0\rangle \langle \nu_{n,2}|0\rangle \cdots \langle \nu_{m,j}|0\rangle \langle \nu_{n,j}|0\rangle \cdots \langle \nu_{m,k}|0\rangle \langle \nu_{n,k}|0\rangle, \quad (9)$$

where $\langle \nu_{m,j}|0\rangle = \sqrt{\frac{S_{m,j}^{\nu_{m,j}} e^{-S_{m,j}}}{\nu_{m,j}!}}$ is the Franck-Condon amplitude. Here $S_{m,j}$ is the Huang-Rhys factor for the j th vibrational mode localized on pigment m . Due to the relatively small Huang-Rhys factors, we only consider the ground state and the first excited vibrational state of the vibrational modes.

Since the vibronic system size increases drastically with the number of modes, a complete treatment is impractical. In general, vibrational modes which are quasi-resonant with excitonic transitions between strongly coupled pigments have the most significant effect on the dynamics. Such modes can invoke fast coherent transport between two vibronic states (usually of the $|m,0\rangle \rightarrow |n,1\rangle$ type). In the literature, the most notable vibrational mode for FMO is that around 180 cm^{-1} which is quasi resonant with the energy gap between various pairs of lowest exciton states. In FMO, for example, there are two independent path ways that lead to the lowest energy exciton localized on BChl 3. They originate from either the low energy exciton that involves a linear combination of sites BChl 1 and 2, or from the exciton that is predominantly localized on BChl 4. Both these pathways have gaps to the exit state BChl3 that are near resonant with the 180 cm^{-1} vibration on this chromophore. From the realistic site-dependent intramolecular spectral densities $J_m^{intra}(\omega)$ it can be seen that the peak associated with this mode is particularly prominent on BChl 3, the proposed linker site to the reaction centre. This potentially suggests its significance to energy transport in FMO. Indeed, enhanced exciton transport in the presence of this mode has been demonstrated²⁹. Since we are only interested in obtaining physical insight rather than an exact picture of the vibronic dynamics, we thus incorporate only this mode in the vibronic Hamiltonian and ignore the rest of the discrete modes, while maintaining the realistic site-dependent spectral density incorporated perturbatively.

To locate this peak on the spectral densities of the other pigments, we first observe that for BChl 3, this peak coincides mostly with a band of closely and almost equally spaced excitonic energy

Table 2 Site-dependent Huang-Rhys factors S_m and vibrational mode frequencies ω_m^{vib} used in this work.

m	S_m (cm^{-1})	ω_m^{vib} (cm^{-1})
1	0.0443	158.52
2	0.0174	173.95
3	0.0634	178.20
4	0.0312	164.90
5	0.0280	161.18
6	0.0433	165.97
7	0.0493	169.16
8	0.0414	173.42
Mean	0.0398	168.16

gaps centred around 168 cm^{-1} in the relevant low-lying excitons. We therefore select the peak closest in frequency to this band of excitonic energy gaps for all the other pigments. Note also that this peak is in fact composed of a cluster of smaller peaks corresponding to closely-spaced vibrational modes. Thus for simplicity, we treat this cluster of modes as one effective vibrational mode with a Huang-Rhys factor S_m obtained by summing up the constituent Huang-Rhys factors, and a frequency ω_m^{vib} equivalent to the frequency of the vibrational peak. It turns out the frequency of this peak averaged over all the sites is around 168 cm^{-1} as well (although it is around 180 cm^{-1} on BChl 3). Thus from this point forward, we will refer to this vibrational mode as the 168 cm^{-1} mode. The computed site-dependent values of S_m and ω_m^{vib} are listed in Table 2.

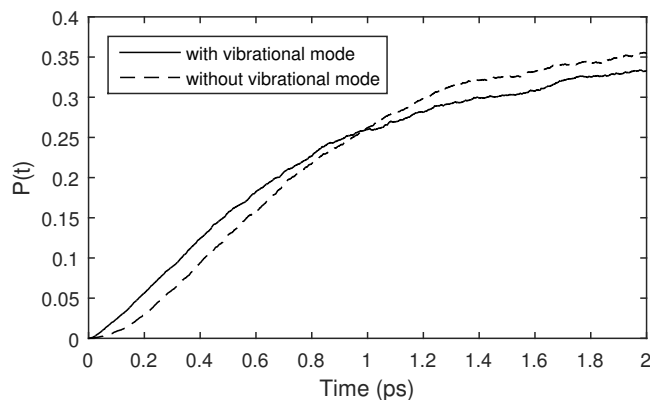
5.1 Optimality of intramolecular electron-phonon coupling

The lowest energy pigment BChl 3 is usually assumed to be coupled to the reaction centre, although in our previous work, referred to above, we also considered the second lowest pigment BChl 4 as a possible target site. However we observe only a deterioration in energy transfer to BChl 4 with the inclusion of the 168 cm^{-1} mode. We now therefore concentrate on the vibronic enhancement observed at BChl 3 (Figure 1), consistent with the findings of Nalbach et. al.²⁹. Interestingly, this enhancement only takes places within 1 ps, which is also the time scale under which long-lived coherence is experimentally-detected. We will therefore only consider exciton dynamics in this time scale for the remainder of this section.

To gauge the optimality of the actual site-dependent intramolecular spectral density configuration, its corresponding energy transfer efficiency is compared to 400 random site-dependent configurations (Figure 2). We define here the measure of energy transfer efficiency as the time-averaged population at BChl 3:

$$\eta = \frac{1}{\tau} \int_0^{\tau} \rho_{33}(t) dt, \quad (10)$$

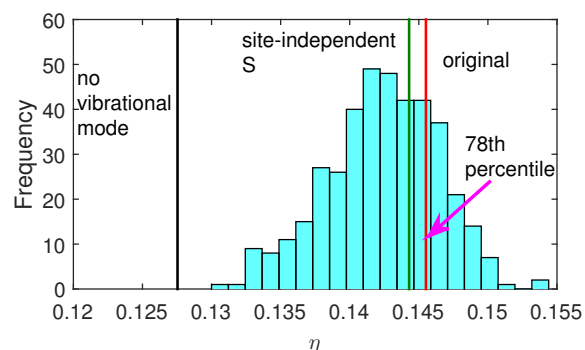
where now $\rho_{33}(t) = \rho_{33,v_3=0}(t) + \rho_{33,v_3=1}(t)$ is the time-dependent total population at BChl 3, taking into account both ground and excited vibrational states. As already mentioned, $\tau = 1 \text{ ps}$. Noting that the intramolecular spectral density is characterized by both

**Fig. 1** Site population dynamics at BChl 3 with and without the inclusion of the near 168 cm^{-1} vibrational mode. The vibronic enhancement is observed only within the time scale of 1 ps after which a deterioration in energy transfer, relative to the purely electronic case, takes place.

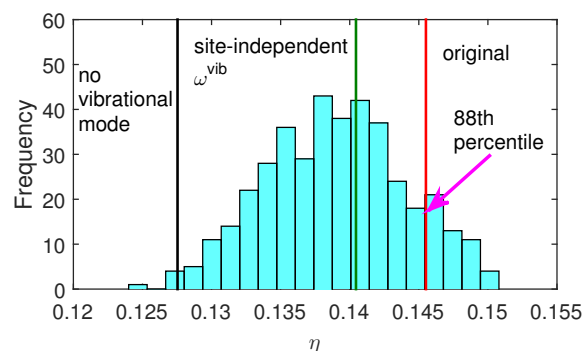
S_m and ω_m^{vib} , the random configurations were obtained for the following scenarios: i) only the S_m configurations were randomized while the ω_m^{vib} configuration remain fixed to that of the original for each realization (Figure 2(a)), ii) only the ω_m^{vib} configurations were randomized while S_m configurations remain fixed to that of the original for each realization (Figure 2(b)) and iii) both S_m and ω_m^{vib} configurations were simultaneously randomized (Figure 2(c)). In each scenario, the randomized site-dependent configurations have the same mean, maximum and minimum values as that of the original for the parameter in question. We also define here a site-independent benchmark where for either S only (case i)), ω^{vib} (case ii)) only or both (case iii)), each site is assigned the mean value of the corresponding parameter from the original configuration. The parameter which is not made site-independent is assigned the corresponding original configuration.

The histograms show that even though the actual λ_m configuration is not the most efficient one, its efficiency in each case nevertheless falls in the upper percentile range (78th to 88th percentile) and surpasses the efficiency for the corresponding site-independent case, suggesting the presence of an underlying optimization mechanism. Note also that within this intramolecular parameter range almost all of the vibronic configurations have improved efficiencies compared to the purely electronic case, indicating robustness.

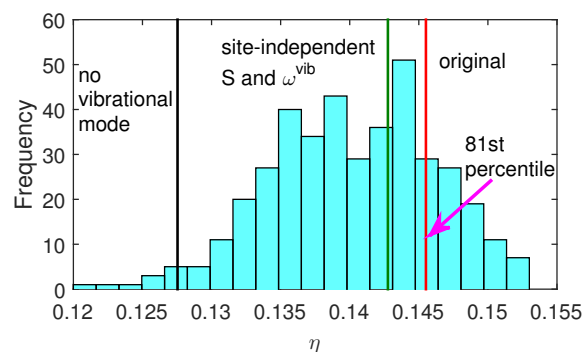
From the outset, the high degree of optimization as observed in Figure 2(a) may not seem too surprising considering the much larger Huang-Rhys factor at the exit site of BChl 3 (Table 2) compared to the other sites. To ascertain if the S_m values of the other pigments also contribute to the optimization observed, we repeated the randomization process in Figure 2(a), with the same constraints on the mean, maximum and minimum values, but with S_3 fixed to the original value. We found that even with this constraint, the efficiency of the original configuration is still above the 50th percentile (66th percentile). The efficiency of the original configuration is also still higher than its site-independent counterpart, although the difference is now much smaller. These observations imply that the S_m values of pigments other than BChl 3 are also configured for optimized energy transport, but a large



(a)



(b)



(c)

Fig. 2 Histogram of efficiencies η for 401 random configurations (including the original) of the intramolecular spectral density where randomization is applied to (a) only S_m , (b) only ω_m^{vib} and (c) both S_m and ω_m^{vib} . All the random configurations have the same mean, maximum and minimum as that of the original. The red, green and black vertical lines represent the original configuration, the corresponding site-independent configuration, and the purely electronic case respectively.

contribution of the optimization comes from S_3 .

6 PC645

Whilst interesting, the inclusion of vibronic modes does not appear to have had too dramatic an effect upon EET in the FMO complex. Let us therefore turn to the phycobiliprotein complex PC645.

Up until now we have employed a single ensemble-averaged electronic Hamiltonian derived from experimental results for FMO. Such an approach is reasonably valid for light-harvesting complexes with rigid chromophores — such as FMO. However for phycobiliproteins found in cryptophyte marine algae, the validity of the ensemble average approach may be questionable. The flexible structure of bilins leads to fluctuations in their electronic properties — notably the energies, and to a lesser extent the interchromophoric couplings. Interestingly, despite the significant system fluctuations, a sufficiently high light-harvesting efficiency is still maintained, suggesting a design principle to ensure robustness may well be in place.

In general, as previously seen, vibrational modes which are quasi-resonant with excitonic transitions between strongly coupled pigments tend to have the most significant effect on the dynamics. Such modes can invoke fast coherent transport between two vibronic states (usually of the $|m, 0\rangle \rightarrow |n, 1\rangle$ type).

The PC645 complex consists of eight light-absorbing bilins of three different types, i.e. MBV_{18A}, MBV_{18B}, DBV_{50C}, DBV_{50D}, PCB_{58C}, PCB_{58D}, PCB_{82C} and PCB_{82D} (Figure 3). This particular set of bilins provides a survival advantage to the cryptophyte algae in two ways. First, it broadens the spectral range available for light-harvesting. Secondly, these bilins absorb sunlight in a different spectral region from that of other plants and most algae (which are usually chlorophyll-based), thus avoiding competition³⁰.

The light-harvesting process in PC645 begins with photoexcitation of the strongly-coupled DBV dimer at the centre of the complex. Unlike the unidirectional funnel of the FMO complex, EET in the PC645 complex is more multidirectional, where the exciton flows out from the core to the peripheral bilins. To facilitate transfer to the reaction centre, the excitation must first be down-converted to the low energy PCB_{82s}, which is more energetically compatible with the chlorophyll-based reaction centre. The down-conversion from the high energy (donor) bilins to the low energy (acceptor) bilins occurs over a significant energy gap ($\approx 1600 \text{ cm}^{-1}$ on average), yet experiments have shown that this energy transfer channel is surprisingly efficient³¹. Since this cannot be explained by a purely electronic transport, it is believed that this down-conversion process is of vibronic nature, where the excess energy is dissipated through the excitation of strongly-coupled intramolecular vibrational modes. Interestingly, there exists a strongly-coupled mode at approximately 1600 cm^{-1} which is particularly prominent on the acceptor PCB_{82s}. Dean et al.³⁰ attributed this down conversion process to a coherent vibronic transport. In fact, most of the work on vibronic transport in light-harvesting complexes have adopted this view. However recent work from the Aspuru-Guzik group^{32,33} proposed that the vibronic transport in PC645 is in fact incoherent, and argued that

such incoherent transport is more robust. Whether a vibronic transition occurs coherently or incoherently depends on factors such as the strength of the system-bath coupling, the magnitude of the vibronic coupling, and the energetic disorder. Generally, weaker system-bath coupling, and a strong or comparable vibronic coupling relative to the vibronic energy gap (i.e. the energy gap between the $|m, 0\rangle$ and $|n, 1\rangle$ states in question) tend to support coherent transport.

The purpose of this work is to investigate the source of the light-harvesting robustness of PC645. Because all prior theoretical investigations on energy transport in PC645 have employed a single ensemble average Hamiltonian, this question has never been properly addressed. Previous theoretical work on PC645 by Blau et. al.³² and Huo et. al.³⁴ used the experimentally-obtained ensemble-averaged site energies from Mirkovic et. al.³⁵. To address this issue, we investigate for the first time, energy transport in PC645 in the presence of varying electronic configurations. Here we propose that the source of the robustness lies in the presence of multiple possible EET pathways — that is, whenever a change in configuration shuts down certain EET pathways, alternative pathways are “activated” in exchange. We argue that these multiple pathway possibilities can be achieved simply through the presence of multiple strongly-coupled intramolecular modes spanning a broad range of frequencies and more than one target site.

7 Numerical procedure for PC645

The investigation was performed on an ensemble of 308 inherent structure configurations of PC645, where each configuration is represented by a different electronic Hamiltonian. The configurations were sampled from Molecular Dynamics trajectories spaced approximately 100 ps apart³⁶. For each ensemble member, we also employ site-dependent spectral densities, also computed using quantum chemistry methods.

In principle, there should be one set of site-dependent intramolecular spectral densities per configuration. However, due to the high computational cost required to compute site-dependent spectral densities for each and every configuration, a different set of spectral densities was calculated only after every 18 — 20 configurations, resulting in only 16 sets of spectral densities altogether. This approach is based on the assumption that there should be little variation in the electron-phonon coupling within a sufficiently short period of time. A more detailed explanation on the computation of the Hamiltonians and intramolecular spectral densities can be found in the Supporting Information of ref.³⁶).

For simplicity, we again employ the Drude-Lorentz regularized Ohmic form to represent the site-dependent spectral density

$$J_m^{DL}(\omega) = 2\lambda_m\Omega_m \frac{\omega}{\omega^2 + \Omega_m^2}, \quad (11)$$

where Ω_m is the cutoff frequency. The same intermolecular spectral density was assigned to each of the 308 configurations. Pairs of chromophores of the same type were assigned the same reorganization energies:

$$\begin{aligned} \text{PCB}_{82C} \text{ and } \text{PCB}_{82D}: & 42.46 \text{ cm}^{-1} \\ \text{PCB}_{58C} \text{ and } \text{PCB}_{58D}: & 53.71 \text{ cm}^{-1} \\ \text{DBV}_{50C} \text{ and } \text{DBV}_{50D}: & 42.45 \text{ cm}^{-1} \\ \text{MBV}_{18A} \text{ and } \text{MBV}_{18B}: & 147.54 \text{ cm}^{-1} \end{aligned}$$

All the chromophores were assigned the same cutoff frequency of 812.5 cm^{-1} . It must be mentioned here that the computation of realistic intermolecular spectral densities is still a work in progress. The bath parameter values assigned here were obtained from averaged values or approximations from preliminary results. Nevertheless, these set of values still reflect the important site variation, notably the much larger reorganization energy for the MBVs. Since we are only interested in investigating the robustness of vibronic EET, these approximate values are not expected to overly affect the key conclusions.

Note also that, as was the case with FMO, the peak in the spectral density associated with our vibronic mode in the PC645 calculations is in fact composed of a cluster of smaller peaks corresponding to closely-spaced vibrational modes. Thus again, we treat this cluster of modes as one effective vibrational mode with a Huang-Rhys factor S_m obtained by summing up the constituent Huang-Rhys factors, and a frequency ω_m^{vib} equivalent to the frequency of the vibrational peak. For the work here, we consider four of the most strongly-coupled intramolecular modes, i.e. the modes around 960 cm^{-1} , 1270 cm^{-1} , 1400 cm^{-1} , 1600 cm^{-1} . However, because the vibronic system size increases drastically with the number of modes, we treat these modes separately, i.e. at each instance, only one of these modes is incorporated into the system Hamiltonian, on each site. The intramolecular spectral densities for PC645 are constructed by Gaussian-broadening the discrete modes. However, the widths are twice that of FMO resulting in many partially resolved neighbouring peaks due to significant overlap between broadened modes. One particular broadened mode can in fact have significant contribution to two neighbouring peaks in the spectral density. This leads to ambiguity in assigning the cluster of modes which contribute to a selected effective peak.

In order to maintain a consistent and efficient assignment over all the different configurations as well as sites, we devised a different approach to extract the intramolecular vibrational frequencies and Huang-Rhys factors. First we note that the strength of the intramolecular electron-phonon coupling is indicated by the height of the peaks in the intramolecular spectral density. This peak height is in turn influenced by both the Huang-Rhys factors of overlapping broadened modes (which determine the height of each broadened mode) as well as the amount of overlap between those modes (which is determined by both the distance between the modes and the degree of broadening). If we instead imagine the particular peak as one effective broadened mode with a height of $h_{m,j}^{eff}$, we can equate $h_{m,j}^{eff}$ to the height of a Gaussian-broadened mode and upon rearranging obtain the corresponding effective reorganization energy:

$$\lambda_{m,j}^{eff} = \sqrt{\frac{2}{\pi}} \frac{h_{m,j}^{eff} \sigma}{\omega_{m,j}^{eff}}, \quad (12)$$

where $\sigma = 14 \text{ cm}^{-1}$ and $\omega_{m,j}^{eff}$ is the frequency of the effective mode j' , which is determined as the frequency of the highest peak in the vicinity of the frequency of interest.

Then from the definition of the Huang-Rhys factor,

$$S_{m,j'}^{eff} = \frac{\lambda_{m,j'}^{eff}}{\omega_{m,j'}^{eff}}, \quad (13)$$

where $S_{m,j'}^{eff}$ is the Huang-Rhys factor of the effective mode. With this approach, our parameters of interest $\omega_{m,j'}^{eff}$ and $S_{m,j'}^{eff}$ can be easily and efficiently computed.

The initial electronic excitation was assigned as localized on DBV_{50D} in the ground vibrational state as in ref.³², while the target sites are the PCB_{82C} and PCB_{82D} bilins^{31–33}. We also assume, as before, that for each pigment m , both the $|m,0\rangle$ and $|m,1\rangle$ states are subjected to the same intermolecular electron-phonon interaction. Finally, numerical computation of the exciton dynamics is performed using the Coherent Modified Redfield Theory (CMRT)^{18,19} for the temperature of 300 K. Physical insight is obtained via statistical analysis of the results.

8 Role of vibronic excitation in PC645

To give an idea of important EET pathways in PC645, we present a schematic of the PC645 structure in Figure 3, where the most significant mean electronic couplings are shown. From Figure 3, we identify six channels with non-negligible electronic coupling between a donor bilin in the upper energy manifold and each of the acceptor PCB_{82s} . These channels are: $\text{DBV}_{50D(C)} \rightarrow \text{PCB}_{82D(C)}$, $\text{MBV}_{18A(B)} \rightarrow \text{PCB}_{82D(C)}$ and $\text{DBV}_{50C(D)} \rightarrow \text{PCB}_{82D(C)}$. Figure 4 shows the distribution of the site energies over the ensemble of 308 configurations. This spread of energies leads to a corresponding distribution of site energy gaps. In particular, both the mode and mean energy gap (which is obviously also the ensemble average energy gap) for the $\text{DBV} \rightarrow \text{PCB}$ channels are in the vicinity of 1600 cm^{-1} .

The observation that a number of these energy gaps are comparable to the frequencies of strongly-coupled intramolecular modes suggests that these channels could potentially participate in vibronic energy transport to the target sites. Note that unlike in the existing literature where only the $\text{DBV core} \rightarrow \text{PCB}$ channel (bridged by the 1600 cm^{-1} mode) is usually considered as the vibronic channel of interest, we also consider the $\text{MBV} \rightarrow \text{PCB}_{82}$ channels due to the different MBV energetic ordering in the unprotonated system used here. That said, we would still expect the $\text{DBV}_{50D(C)} \rightarrow \text{PCB}_{82D(C)}$ channels to be the dominant contributor to vibronic EET, taking into account the strength of the electronic coupling, the overlap between the distribution of energy gaps and the frequencies of the intramolecular modes and the fact that this channel enables direct exciton transfer from the source to the target site.

The absence of strongly-coupled modes with frequencies over 1700 cm^{-1} suggests that intramolecular modes with frequencies higher than that are unnecessary for EET for all or at least most of the accessible PC645 configurations. Interestingly, there is significant dispersion in the energy gaps which can be as large as 3000

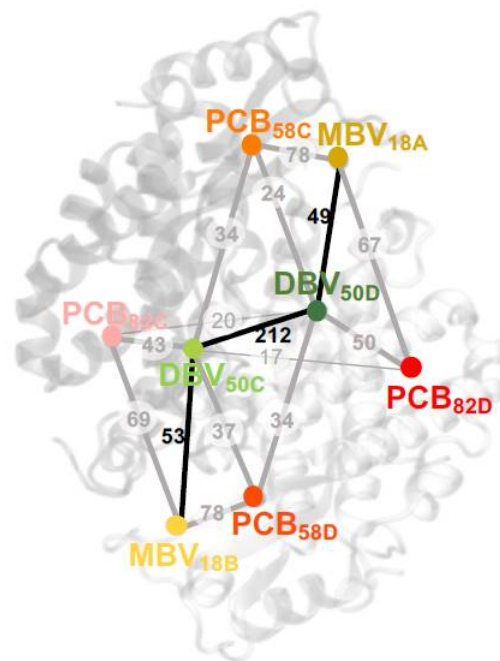


Fig. 3 PC645 structure showing the mean absolute values of electronic couplings, to provide a general guideline of typical EET pathways and exciton delocalization in PC645. Taken from ref.³⁶. Strong couplings are denoted by thick lines and weak couplings by thin lines. Electronic couplings between two pigments which are of comparable magnitude to the corresponding site energy difference are indicated by black lines. Such a scenario can support exciton delocalization between the two pigments in question. Electronic couplings which are an order of magnitude smaller than their corresponding site energy differences are represented by grey lines. In these situations, exciton delocalization over the pigments in question is not possible, unless a bridging vibrational mode is present.

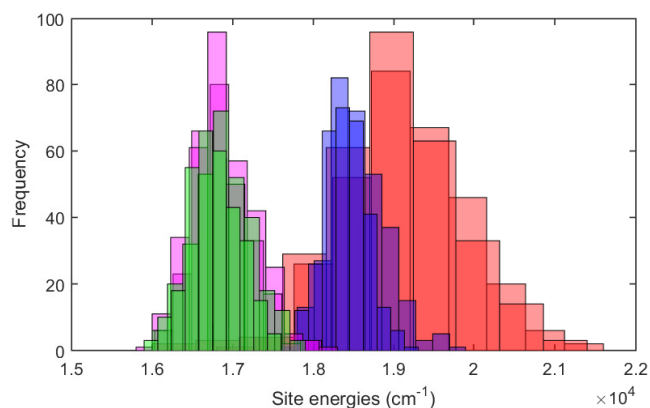


Fig. 4 Distribution of site energies of PC645 over 308 configurations. Histograms are coloured according to chromophore type — MBVs: red, DBVs: blue, PCB_{82s} : magenta, PCB_{82s} : green. Note that the site energies here are the “actual” site energies, and not the site energies taken relative to the lowest site energy of each configuration.

— 4000 cm^{-1} . These large energy gaps may at first seem unbridgeable with the available intramolecular modes. However, it could be that the contribution of these unbridgeable energy gaps becomes statistically insignificant due to the presence of multiple possible EET pathways, as well as the shape of the energy gap distribution (i.e. symmetrical distribution about the mean, with extreme energy gaps being much less probable than intermediate ones). In other words, most of the configurations are likely to have at least one pathway where the energy gaps are small enough to be bridgeable by existing intramolecular modes, or able to support purely electronic transport. Indeed, when we checked the energy gaps of the six channels mentioned above for the ensemble of configurations, we found that approximately 99% of the configurations have at least one channel with an energy gap below 2000 cm^{-1} . Even if only the two dominant channels, $\text{DBV}_{50D} \rightarrow \text{PCB}_{82D}$ and $\text{DBV}_{50C} \rightarrow \text{PCB}_{82C}$ are considered, around 96% of the configurations have at least one energy gap which is smaller than 2000 cm^{-1} (75% and 83% respectively if only one of them is considered).

8.1 Multiple possible EET pathways as a source of robustness

First we quantify the EET efficiency for each ensemble member as the average total population at the target sites within $\tau = 1$ ps:

$$\eta = \frac{1}{\tau} \int_0^{\tau} P_{82}(t) dt, \quad (14)$$

where $P_{82}(t) = P_{82C,v=0}(t) + P_{82C,v=1}(t) + P_{82D,v=0}(t) + P_{82D,v=1}(t)$ is the time-dependent total population at the two PCB_{82} bilins, taking into account both the excited and unexcited vibrational states.

Figure 5(a) depicts the η distribution of the 308 configurations in the absence of intramolecular vibrational modes. As we can see, the efficiency of the purely electronic EET is generally poor — the distribution is positively skewed with a large proportion of the configurations with $\eta < 0.05$ and no configurations with η exceeding 0.2. The mean η of the ensemble is only 0.0355 while the efficiency of the ensemble-averaged configuration is even lower with $\eta = 0.0092$. In contrast, we observe statistical improvement in η (as reflected by the range, mean and mode of the distribution) in the presence of strongly-coupled intramolecular modes, for each of the four vibrational modes investigated in this work. The η distributions resulting from incorporating a single intramolecular mode on each site are presented in Figures 5(b) and (c) for the case of the 1400 cm^{-1} and 1600 cm^{-1} modes respectively. Nevertheless, the skewness in the η distribution is still present. In comparison, the η distribution appears somewhat symmetrical if we select only the best η obtained from among the four intramolecular modes (Figure 5(d)). We observe a significantly improved distribution mode ($\eta \approx 0.25$) and wider range, with η reaching as high as approximately 0.6. Both the mean and ensemble average η are also larger than 0.1 (0.2459 and 0.1537 respectively). Inspection of the data reveals that nearly all of the configurations experience improvement in η with approximately 88% of the configurations having $\eta > 0.1$. These obser-

vations suggest that due to the vastly changing energy gaps of PC645 from configuration to configuration, the presence of multiple bridging intramolecular modes spanning a broad range of frequencies may be necessary to ensure that at each instance, at least one vibronic channel can effectively participate in EET.

It is also interesting to note that the best ensemble average and mean η is achieved for the 1400 cm^{-1} mode, and not for the frequently-mentioned 1600 cm^{-1} mode. This is perhaps not too surprising — considering the DBV dimer is delocalized in many of the configurations as well as the ensemble average configuration, it may be more appropriate to view resonance in terms of the excitonic basis (although the site basis should still be able to provide a general guide). For the ensemble average configuration, we notice that the excitonic gaps between the lower energy DBV exciton (exciton 5) and each of the PCB_{82s} are in fact approximately 1400 cm^{-1} .

9 Conclusions

To summarize, we have presented here a summary of our analysis of the importance of site-dependent coupling to the environment in FMO and PC645 and also the role of vibronic modes in the efficiency of EET in these complexes. Given that the coherences that generated so much excitement, and its associated quantum nature, appear to be associated with these vibronic excitations, their role in the energy transfer process is important if we are to claim there is any import in quantum processes in these biological systems. We've reviewed our analysis which indicates FMO seems to have evolved to have optimised the coupling of chromophores to the environment to enhance both coherent and incoherent transport to sites proximal to the reaction centre and have noted some, but not dramatic, enhancement of EET through the inclusion of vibronic modes.

More significantly, we have investigated for the first time, energy transport in the PC645 complex while accounting for the varying electronic configuration (and corresponding intramolecular electron-phonon couplings). To this end, we have performed numerical calculations on a large ensemble of possible PC645 configurations, computed via quantum chemistry methods, to obtain the statistics of EET efficiencies and other relevant parameters.

We addressed the important question of how this flexible light-harvesting complex can maintain EET robustness despite possessing an electronic configuration that changes fairly rapidly with time, sometimes significantly, in particular with regards to the energies and corresponding energy gaps. For future research, it would be interesting to explore if the PC645 structure with its dimer core, symmetrical configuration, and multidirectional energy flow, could perhaps be a design principle to facilitate such robustness, as opposed to say, complexes with a more directed energy flow such as FMO. Incidentally, such structure is quite common in phycobiliproteins.

Conflicts of interest

There are no conflicts to declare.

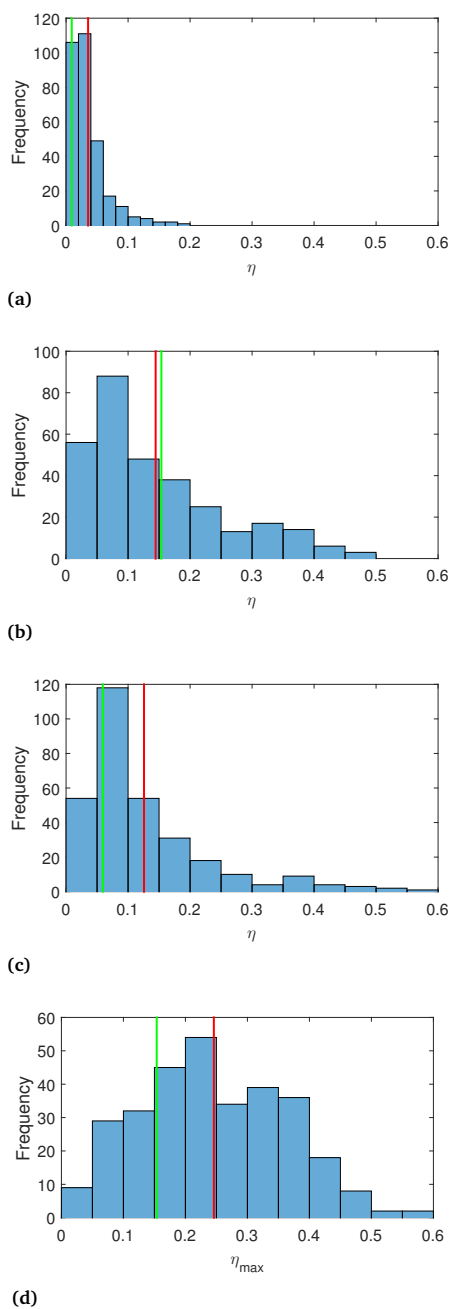


Fig. 5 Distribution of efficiencies η for the configuration-dependent ensemble of PC645 in the absence of intramolecular modes (a), and with the inclusion of a single intramolecular mode with frequency around 1400 cm^{-1} (b) and 1600 cm^{-1} (c) on each site; (d) Distribution of η_{\max} , i.e. the largest η obtained from including any of the four vibrational modes ($\approx 960\text{ cm}^{-1}$, 1270 cm^{-1} , 1400 cm^{-1} or 1600 cm^{-1}). Red and green vertical lines represent the mean and ensemble average η or η_{\max} respectively.

Acknowledgements

DAWH would like to thank Merton College for their support and hospitality through a Visiting Research Fellowship during a significant element of this work. We would like to thank Mi Kyung Lee for access to her data. In particular, we relied completely on her molecular dynamics calculations for the structure and spectra of PC645. DFC gratefully acknowledges support for this research from the US National Science Foundation under Grant No. CHE-1665367.

References

- 1 G. S. Engel, T. R. Calhoun, E. L. Read, T.-K. Ahn, T. Mančal, Y.-C. Cheng, R. E. Blankenship and G. R. Fleming, *Nature*, 2007, **446**, 782–786.
- 2 G. Panitchayangkoon, D. Hayes, K. A. Fransted, J. R. Caram, E. Harel, J. Wen, R. E. Blankenship and G. S. Engel, *Proceedings of the National Academy of Sciences*, 2010, **107**, 12766–12770.
- 3 H. Lee, Y.-C. Cheng and G. R. Fleming, *Science*, 2007, **316**, 1462–1465.
- 4 T. R. Calhoun, N. S. Ginsberg, G. S. Schlau-Cohen, Y.-C. Cheng, M. Ballottari, R. Bassi and G. R. Fleming, *The Journal of Physical Chemistry B*, 2009, **113**, 16291–16295.
- 5 E. Collini, C. Y. Wong, K. E. Wilk, P. M. Curmi, P. Brumer and G. D. Scholes, *Nature*, 2010, **463**, 644–647.
- 6 C. Y. Wong, R. M. Alvey, D. B. Turner, K. E. Wilk, D. A. Bryant, P. M. Curmi, R. J. Silbey and G. D. Scholes, *Nature Chemistry*, 2012, **4**, 396–404.
- 7 E. Romero, R. Augulis, V. I. Novoderezhkin, M. Ferretti, J. Thieme, D. Zigmantas and R. Van Grondelle, *Nature Physics*, 2014, **10**, 676–682.
- 8 N. Christensson, H. F. Kauffmann, T. Pullerits and T. Mančal, *The Journal of Physical Chemistry B*, 2012, **116**, 7449–7454.
- 9 A. Chin, J. Prior, R. Rosenbach, F. Caycedo-Soler, S. Huelga and M. B. Plenio, *Nature Physics*, 2013, **9**, 113–118.
- 10 V. Tiwari, W. K. Peters and D. M. Jonas, *Proceedings of the National Academy of Sciences*, 2013, **110**, 1203–1208.
- 11 M. B. Plenio, J. Almeida and S. Huelga, *The Journal of Chemical Physics*, 2013, **139**, 235102.
- 12 F. Novelli, A. Nazir, G. H. Richards, A. Roozbeh, K. E. Wilk, P. M. Curmi and J. A. Davis, *The Journal of Physical Chemistry Letters*, 2015, **6**, 4573–4580.
- 13 A. Chenu, N. Christensson, H. F. Kauffmann and T. Mančal, *Scientific Reports*, 2013, **3**, 2029.
- 14 R. Stones and A. Olaya-Castro, *Chem*, 2016, **1**, 822–824.
- 15 S. A. Oh, D. F. Coker and D. A. W. Hutchinson, *J. Chem. Phys.*, 2019, **150**, 085102.
- 16 J. Moix, J. Wu, P. Huo, D. Coker and J. Cao, *The Journal of Physical Chemistry Letters*, 2011, **2**, 3045–3052.
- 17 W. M. Zhang, T. Meier, V. Chernyak and S. Mukamel, *The Journal of Chemical Physics*, 1998, **108**, 7763–7774.
- 18 Y.-H. Hwang-Fu, W. Chen and Y.-C. Cheng, *Chemical Physics*, 2015, **447**, 46–53.
- 19 Y. Chang and Y.-C. Cheng, *The Journal of Chemical Physics*,

- 2015, **142**, 034109.
- 20 Q. Ai, Y.-J. Fan, B.-Y. Jin and Y.-C. Cheng, *New Journal of Physics*, 2014, **16**, 053033.
- 21 M.-J. Tao, Q. Ai, F.-G. Deng and Y.-C. Cheng, *Scientific Reports*, 2016, **6**, 27535.
- 22 M. Yang and G. R. Fleming, *Chemical Physics*, 2002, **282**, 163–180.
- 23 J. Piilo, S. Maniscalco, K. Härkönen and K.-A. Suominen, *Physical Review Letters*, 2008, **100**, 180402.
- 24 J. Piilo, K. Härkönen, S. Maniscalco and K.-A. Suominen, *Physical Review A*, 2009, **79**, 062112.
- 25 S. Mukamel, *Principles of Nonlinear Optical Spectroscopy*, Oxford University Press New York, 1995, vol. 29.
- 26 J. M. Womick and A. M. Moran, *The Journal of Physical Chemistry B*, 2011, **115**, 1347–1356.
- 27 T. D. Holstein, *Annals of Physics*, 1959, **8**, 325–342.
- 28 F. C. Spano, *Accounts of Chemical Research*, 2009, **43**, 429–439.
- 29 P. Nalbach, C. Mujica-Martinez and M. Thorwart, *Physical Review E*, 2015, **91**, 022706.
- 30 J. C. Dean, T. Mirkovic, Z. S. Toa, D. G. Oblinsky and G. D. Scholes, *Chem*, 2016, **1**, 858–872.
- 31 A. Marin, A. B. Doust, G. D. Scholes, K. E. Wilk, P. M. Curmi, I. H. van Stokkum and R. van Grondelle, *Biophysical Journal*, 2011, **101**, 1004–1013.
- 32 S. M. Blau, D. I. Bennett, C. Kreisbeck, G. D. Scholes and A. Aspuru-Guzik, *Proceedings of the National Academy of Sciences*, 2018, **115**, E3342–E3350.
- 33 D. I. Bennett, P. Maly, C. Kreisbeck, R. van Grondelle and A. Aspuru-Guzik, *The Journal of Physical Chemistry Letters*, 2018, **9**, 2665–2670.
- 34 P. Huo and D. F. Coker, *The Journal of Physical Chemistry Letters*, 2011, **2**, 825–833.
- 35 T. Mirkovic, A. B. Doust, J. Kim, K. E. Wilk, C. Curutchet, B. Mennucci, R. Cammi, P. M. Curmi and G. D. Scholes, *Photochemical & Photobiological Sciences*, 2007, **6**, 964–975.
- 36 M. K. Lee, K. B. Bravaya and D. F. Coker, *Journal of the American Chemical Society*, 2017, **139**, 7803–7814.